Pergamon

Acta mater. Vol. 46, No. 5, pp. 1719–1729, 1998

Printed in Great Britain
PII: S1359-6454(97)00335-2
1359-6454/98 $19.00 + 0.00

COMPUTER SIMULATION OF ATOMIC ORDERING AND COMPOSITIONAL CLUSTERING IN THE PSEUDOBINARY Ni_3Al–Ni_3V SYSTEM

R. PODURI and L.-Q. CHEN

Department of Materials Science and Engineering, The Pennsylvania State University, University Park, PA 16802, U.S.A.

(Received 8 April 1997; accepted 5 September 1997)

Abstract—The kinetics of diffusional phase transformations in the pseudobinary Ni_3Al–Ni_3V system were studied using a computer simulation technique based on microscope diffusion equations. Our focus is on the initial stages of atomic ordering and compositional clustering process during the phase transformation of an initially homogeneous disordered f.c.c. ternary alloy ($Ni_{75}Al_{25-x}V_x$) into a two-phase mixture of $L1_2$ (Ni_3Al) and DO_{22} (Ni_3V) ordered phases. A thermodynamic model is proposed to describe the phase equilibria in this pseudobinary system. Our computer simulations demonstrated that at small vanadium content, the $L1_2$ ordered domains appear first, followed by the nucleation of DO_{22} ordered domains at the antiphase domain boundaries of $L1_2$, whereas at large vanadium content, precipitation of DO_{22} precedes $L1_2$ domain formation. The simulation results are discussed employing the thermodynamic stability analysis. The ordering and clustering kinetics predicted from our computer simulation are consistent with recent experimental observations. © *1998 Acta Metallurgica Inc.*

1. INTRODUCTION

The pseudobinary Ni_3Al–Ni_3V section of the Ni–Al–V ternary phase diagram was found to contain a eutectoid reaction at temperature, 1281 K, and composition, Ni–5Al–20V (at.%), in which the high-temperature disordered phase, α_1, is at equilibrium with low-temperature $L1_2$ (Ni_3Al) and DO_{22} (Ni_3V) phases [1]. Therefore, a quenched high-temperature disordered phase annealed at low temperatures will transform to a two-phase mixture of $L1_2$ and DO_{22} ordered phases.

Recent transmission electron microscopy (TEM) observations and X-ray diffraction measurements by Bendersky *et al.* [2], demonstrated that the precipitation of $L1_2$ and DO_{22} ordered phases from a disordered matrix with composition Ni–4.5Al–22V, is a rather complicated process involving several intermediate two-phase microstructures, leading to the final eutectoid morphology. Based on these experimental observations, they summarized the entire process in four stages. In stage I, $L1_2$ clusters nucleate coherently in the disordered f.c.c. matrix, followed by stage II, the formation of three different variants of the DO_{22} phase from the remaining disordered matrix accompanied by the transformation of $L1_2$ clusters into cuboidal precipitates. Stage III involves the formation of twins or tetragonal straining of the $L1_2$ phase due to the accommodation of misfit strains and other incompatibilities between the different phases. And finally, in stage IV, a discontinuous coarsening process takes place, leading to a eutectoid lamellar mixture.

The main objective of this paper is to theoretically investigate the sequence of order–disorder transformations and compositional phase separation resulting in the precipitation of $L1_2$ and DO_{22} ordered phases from a disordered matrix in $Ni_{75}Al_{25-x}V_x$, where x is the atom percent of vanadium. It should be pointed out that, as far as the authors are aware, this is the first time that the kinetics of precipitation of two ordered phase from a disordered matrix have been studied theoretically, particularly using computer simulations. The focus will be on the initial stages of precipitation process, i.e. the ordering and phase separation kinetics of $L1_2$ and DO_{22} in a f.c.c. disordered matrix (stages I and II). The results obtained from our computer simulations are interpreted using the thermodynamic stability analysis [3]. For simplicity, we will ignore the effect of elastic strain energy on the two-phase morphology. Our theoretical predictions will be compared with experimental observations by Bendersky *et al.* [2] on the same alloys.

2. COMPUTER SIMULATION MODEL

To investigate the kinetics of diffusional processes in the pseudobinary Ni_3Al–Ni_3V, we employed a computer simulation model recently developed for ternary alloys [4] based on the Önsager-type microscope diffusion equations first proposed by Khachaturyan [5]. In this model, the atomic configurations and the morphologies of a ternary alloy are described by single-site occupation probability

functions $P_A(\mathbf{r},t)$, $P_B(\mathbf{r},t)$ and $P_C(\mathbf{r},t)$ which represent the probabilities of finding an A, B or C atom at a given lattice site $\mathbf{r}$ at a given time t, respectively. At very high temperatures, the equilibrium state of a ternary system corresponds to a homogenous disordered state described by $P_\alpha(\mathbf{r},t) = c_\alpha$ where c_α is the overall composition for component α. When such a homogenous phase is quenched to low temperatures, it will become unstable with respect to atomic ordering, or compositional clustering, or both, depending on the interatomic interactions within the system. The evolution of the initially unstable state to a stable one is a highly non-linear and complex process. It is assumed that such a process may be described by the Önsager-type microscopic diffusion equations as proposed by Khatchaturyan [5]. Since for ternary systems $P_A(\mathbf{r},t) + P_B(\mathbf{r},t) + P_C(\mathbf{r},t) = 1.0$, only two equations are independent at each lattice site. If one assumes the independent variables are $P_A(\mathbf{r},t)$ and $P_B(\mathbf{r},t)$, there will be two independent kinetic equations at each lattice site for species A and B, respectively. Then, one can write the microscopic kinetic equations for ternary systems as

$$\frac{dP_A(\mathbf{r},t)}{dt} = \frac{1}{k_B T}\sum_{r'}\left[L_{AA}(\mathbf{r}-\mathbf{r}')\frac{\delta F}{\delta P_A(\mathbf{r}',t)} + L_{AB}(\mathbf{r}-\mathbf{r}')\frac{\delta F}{\delta P_B(\mathbf{r}',t)}\right]$$

and

$$\frac{dP_B(\mathbf{r},t)}{dt} = \frac{1}{k_B T}\sum_{r'}\left[L_{BA}(\mathbf{r}-\mathbf{r}')\frac{\delta F}{\delta P_A(\mathbf{r}',t)} + L_{BB}(\mathbf{r}-\mathbf{r}')\frac{\delta F}{\delta P_B(\mathbf{r}',t)}\right] \quad (1)$$

where k_B is the Boltzmann constant, T is the temperature, $L_{\alpha\beta}(\mathbf{r}-\mathbf{r}')$ are the exchange probabilities between a pair of atoms, α and β, at lattice site $\mathbf{r}$ and $\mathbf{r}'$ per unit time, and F is the total Helmholtz free energy of the system. In the single-site approximation, the free energy F for a ternary system is given by

$$\begin{aligned}F = &-\frac{1}{2}\sum_{\mathbf{r}}\sum_{\mathbf{r}'}\left[V_{AB}(\mathbf{r}-\mathbf{r}')P_A(\mathbf{r})P_B(\mathbf{r}')\right.\\ &\left.+V_{BC}(\mathbf{r}-\mathbf{r}')P_B(\mathbf{r})P_C(\mathbf{r}')+V_{AC}(\mathbf{r}-\mathbf{r}')P_A(\mathbf{r})P_C(\mathbf{r}')\right]\\ &+k_B T\sum_{\mathbf{r}}\left[P_A(\mathbf{r})\ln(P_A(\mathbf{r}))+P_B(\mathbf{r})\ln(P_B(\mathbf{r}))\right.\\ &\left.+P_C(\mathbf{r})\ln(P_C(\mathbf{r}))\right] \quad (2)\end{aligned}$$

and

$$\begin{aligned}V_{AB}(\mathbf{r}-\mathbf{r}') &= W_{AA}(\mathbf{r}-\mathbf{r}')+W_{BB}(\mathbf{r}-\mathbf{r}')-2W_{AB}(\mathbf{r}-\mathbf{r}')\\ V_{BC}(\mathbf{r}-\mathbf{r}') &= W_{BB}(\mathbf{r}-\mathbf{r}')+W_{CC}(\mathbf{r}-\mathbf{r}')-2W_{BC}(\mathbf{r}-\mathbf{r}')\\ V_{AC}(\mathbf{r}-\mathbf{r}') &= W_{AA}(\mathbf{r}-\mathbf{r}')+W_{CC}(\mathbf{r}-\mathbf{r}')-2W_{AC}(\mathbf{r}-\mathbf{r}')\end{aligned} \quad (3)$$

in which $W_{\alpha\beta}(\mathbf{r}-\mathbf{r}')$ are the pairwise interaction energies between a pair of atoms, α and β (= A, B, or C), at lattice site $\mathbf{r}$ and $\mathbf{r}'$.

One can eliminate $P_C(\mathbf{r},t)$ in the free energy expression by substituting $P_C(\mathbf{r},t)$ with $1 - P_A(\mathbf{r},t) - P_B(\mathbf{r},t)$ and ignoring terms which do not depend on the inhomogeneous distribution of single-site occupation probability functions,

$$\begin{aligned}F = &-\frac{1}{2}\sum_{\mathbf{r}}\sum_{\mathbf{r}'}\left[(-V_{AB}(\mathbf{r}-\mathbf{r}')+V_{BC}(\mathbf{r}-\mathbf{r}')\right.\\ &+V_{AC}(\mathbf{r}-\mathbf{r}'))P_A(\mathbf{r})P_B(\mathbf{r}')+V_{AC}(\mathbf{r}-\mathbf{r}')P_A(\mathbf{r})P_A(\mathbf{r}')\\ &\left.+V_{BC}(\mathbf{r}-\mathbf{r}')P_B(\mathbf{r})P_B(\mathbf{r}')\right]\\ &+k_B T\sum_{\mathbf{r}}\left[P_A(\mathbf{r})\ln(P_A(\mathbf{r}))+P_B(\mathbf{r})\ln(P_B(\mathbf{r}))\right.\\ &\left.+(1-P_A(\mathbf{r})-P_B(\mathbf{r}))\ln(1-P_A(\mathbf{r})-P_B(\mathbf{r}))\right] \quad (4)\end{aligned}$$

The variational derivatives in the kinetic equation (1) can then be written as

$$\begin{aligned}\frac{\delta F}{\delta P_A(\mathbf{r}')} = &\frac{1}{2}\sum_{r}\left[(-V_{AB}(\mathbf{r}-\mathbf{r}')+V_{BC}(\mathbf{r}-\mathbf{r}')\right.\\ &\left.+V_{AC}(\mathbf{r}-\mathbf{r}'))\right]P_B(\mathbf{r})\\ &+\sum_{\mathbf{r}}V_{AC}(\mathbf{r}-\mathbf{r}')P_A(\mathbf{r})\\ &+k_B T\ln\left[\frac{P_A(\mathbf{r}')}{(1-P_A(\mathbf{r}')-P_B(\mathbf{r}'))}\right] \quad (5)\end{aligned}$$

and

$$\begin{aligned}\frac{\delta F}{\delta P_B(\mathbf{r}')} = &\frac{1}{2}\sum_{r}\left[(-V_{AB}(\mathbf{r}-\mathbf{r}')+V_{BC}(\mathbf{r}-\mathbf{r}')\right.\\ &\left.+V_{AC}(\mathbf{r}-\mathbf{r}'))\right]P_A(\mathbf{r})\\ &+\sum_{\mathbf{r}}V_{BC}(\mathbf{r}-\mathbf{r}')P_B(\mathbf{r})\\ &+k_B T\ln\left[\frac{P_B(\mathbf{r}')}{(1-P_A(\mathbf{r}')-P_B(\mathbf{r}'))}\right]\end{aligned}$$

Since the total numbers of A, B and C atoms are fixed, one has the condition

$$\sum_{\mathbf{r}}\frac{dP_\alpha(\mathbf{r})}{dt} = \frac{dN_\alpha}{dt} = 0 \quad (6)$$

where N_α is the total number of α (= A, B or C) atoms in the system. Equation (6) implies that

$$\sum_{\mathbf{r}}L_{\alpha\beta}(\mathbf{r}) = 0, \alpha, \beta = \text{A or B} \quad (7)$$

3. THERMODYNAMIC MODEL FOR THE Ni_3Al–Ni_3V PSEUDOBINARY SYSTEM

According to experimental observations, there are two ordered phases which appear in the Ni_3Al–Ni_3V pseudobinary phase diagram, namely $L1_2$ and

DO_{22}. To obtain the free energies of the high-temperature disordered phase and the low temperature ordered phases, the single-site occupation probabilities in the free energy model are replaced by composition and corresponding long-range order parameters. For an $L1_2$ ordered phase, the occupation probabilities are given by [5]

$$\begin{aligned} P_A(\mathbf{r}) &= c_A(1+\eta_{1A}(e^{2\pi ix}+e^{2\pi iy}+e^{2\pi iz})) \\ P_B(\mathbf{r}) &= c_B(1+\eta_{1B}(e^{2\pi ix}+e^{2\pi iy}+e^{2\pi iz})) \end{aligned} \tag{8}$$

where c_A and c_B are the average compositions of A and B in the ternary Ni–Al–V system, η_{1A} and η_{1B} represent the long-range order parameters which are proportional to the concentration amplitudes for component A and B, respectively, in the $L1_2$ ordered phase, and x, y and z are the fractional Cartesian coordinates of lattice positions in terms of the respective lattice parameters of the f.c.c. unit cell. It is easy to see that the occupation probabilities assume only two values $c + 3c\eta_1$ and $c - c\eta_1$ on an f.c.c. lattice. Substituting (8) into the free energy expression (4), we have the free energy of the $L1_2$ ordered phase per atom as a function of composition and long-range order parameters,

$$\begin{aligned} F(L1_2) =& 1/2\big[(V_{BC}(\mathbf{0})+V_{AC}(\mathbf{0})-V_{AB}(\mathbf{0}))c_Ac_B \\ &+ V_{BC}(\mathbf{0})c_B^2+V_{AC}(\mathbf{0})c_A^2\big] \\ &+ (3/2)\big[\eta_{1A}^2V_{AC}(\mathbf{k}_1)+\eta_{1B}^2V_{BC}(\mathbf{k}_1) \\ &+ \eta_{1A}\eta_{1B}(V_{BC}(\mathbf{k}_1)+V_{AC}(\mathbf{k}_1)-V_{AB}(\mathbf{k}_1))\big] \\ &+ (k_BT/4)\big[c_A(1+3\eta_{1A})\ln(c_A(1+3\eta_{1A})) \\ &+ c_B(1+3\eta_{1B})\ln(c_B(1+3\eta_{1B})) \\ &+ (1-c_A(1+3\eta_{1A})-c_B(1+3\eta_{1B})) \\ &\quad \ln(1-c_A(1+3\eta_{1A})-c_B(1+3\eta_{1B}))\big] \\ &+ (3k_BT/4)\big[c_A(1-\eta_{1A})\ln(c_A(1-\eta_{1A})) \\ &+ c_B(1-\eta_{1B})\ln(c_B(1-\eta_{1B})) \\ &+ (1-c_A(1-\eta_{1A})-c_B(1-\eta_{1B})) \\ &\quad \ln(1-c_A(1-\eta_{1A})-c_B(1-\eta_{1B}))\big] \end{aligned} \tag{9}$$

where $V_{\alpha\beta}(0)$ and $V_{\alpha\beta}(\mathbf{k}_1)$ are the values of the Fourier transform, $V_{\alpha\beta}(\mathbf{k})$, of $V_{\alpha\beta}(\mathbf{r})$, at $\mathbf{k} = 0$ and $\mathbf{k} = \mathbf{k}_1$, and $V_{\alpha\beta}(\mathbf{k})$, for the an f.c.c. lattice, is given by

$$\begin{aligned} V_{\alpha\beta}(\mathbf{k}) =& 4V_{\alpha\beta}^1(\cos\pi h\cdot\cos\pi k+\cos\pi h\cdot\cos\pi l \\ &+ \cos\pi k\cdot\cos\pi l) \\ &+ 2V_{\alpha\beta}^2(\cos 2\pi h+\cos 2\pi k+\cos 2\pi l) \\ &+ 8V_{\alpha\beta}^3(\cos 2\pi h\cdot\cos\pi k\cdot\cos\pi l+\cos\pi h \\ &\quad \cdot\cos 2\pi k\cdot\cos\pi l+\cos\pi h\cdot\cos\pi k\cdot\cos 2\pi l) \\ &+ 4V_{\alpha\beta}^4(\cos 2\pi h\cdot\cos 2\pi k+\cos 2\pi h\cdot\cos 2\pi l \\ &+ \cos 2\pi k\cdot\cos 2\pi l) \\ &+ \dots \end{aligned} \tag{10}$$

where $V_{\alpha\beta}^1$, $V_{\alpha\beta}^2,\dots$, $V_{\alpha\beta}^i$, are the first-, second-, and ith-nearest neighbor effective interchange interaction energies between α and β atoms, respectively, and h, k and l are integers related to the reciprocal lattice through

$$\mathbf{k} = (k_x, k_y, k_z) = 2\pi(h\mathbf{a}_1^* + k\mathbf{a}_2^* + l\mathbf{a}_3^*) \tag{11}$$

with $\mathbf{a}_1^*$, $\mathbf{a}_2^*$ and $\mathbf{a}_3^*$ being the unit reciprocal lattice vectors of the f.c.c. lattice along [100], [010] and [001] directions, respectively, and $|\mathbf{a}_1^*| = |\mathbf{a}^*{}_2| = |\mathbf{a}_3^*| = 1/a_0$ (a_0 is the lattice parameter of the f.c.c. lattice); $\mathbf{k_1} = 2\pi\mathbf{a}_1^*$ is the superlattice vector for the $L1_2$ ordered phase.

For a DO_{22} ordered phase, the occupation probabilities can be written as

$$\begin{aligned} P_A(\mathbf{r}) &= c_A(1+\eta_{2A}e^{2(2x+z)}+2\eta_{3A}\cos\pi(2x+z)) \\ P_B(\mathbf{r}) &= c_B(1+\eta_{2B}e^{2(2x+z)}+2\eta_{3B}\cos\pi(2x+z)) \end{aligned} \tag{12}$$

where η_{2A}, η_{3A}, η_{2B} and η_{3B} are order parameters which are proportional to the amplitudes of the concentration waves of respective A and B atomic species in the DO_{22} ordered phase. On an f.c.c. lattice, these probabilities take three values, $c + c\eta_2 + 2c\eta_3$, $c + c\eta_2 - 2c\eta_3$ and $c - c\eta_2$. By substituting (11) into the free energy expression (4), we obtain the free energy per atom of the DO_{22} phases as a function of composition and order parameters,

$$\begin{aligned} F(DO_{22}) =& 1/2\big[(V_{BC}(\mathbf{0})+V_{AC}(\mathbf{0})-V_{AB}(\mathbf{0}))c_Ac_B \\ &+ V_{BC}(\mathbf{0})c_B^2+V_{AC}(\mathbf{0})c_A^2\big] \\ &+ (1/2)(\eta_{2A}^2V_{AC}(2\mathbf{k}_2)+\eta_{2B}^2V_{BC}(2\mathbf{k}_2) \\ &+ \eta_{2A}\eta_{2B}(V_{BC}(2\mathbf{k}_2)+V_{AC}(2\mathbf{k}_2)-V_{AB}(2\mathbf{k}_2)) \\ &+ 2\eta_{3A}^2V_{AC}(\mathbf{k}_2)+2\eta_{3B}^2V_{BC}(\mathbf{k}_2) \\ &+ 2\eta_{3A}\eta_{3B}(V_{BC}(\mathbf{k}_2)+V_{AC}(\mathbf{k}_2)-V_{AB}(\mathbf{k}_2)) \\ &+ (k_BT/4)\big[c_A(1+\eta_{2A} \\ &+ 2\eta_{3A})\ln c_A(1+\eta_{2A}+2\eta_{3A}) \\ &+ c_B(1+\eta_{2B}+2\eta_{3B})\ln c_B(1+\eta_{2B}+2\eta_{3B}) \\ &+ (1-c_A(1+\eta_{2A}+2\eta_{3A}) \\ &- c_B(1+\eta_{2B}+2\eta_{3B}))\ln(1-c_A(1+\eta_{2A} \\ &+ 2\eta_{3A})-c_B(1+\eta_{2B}+2\eta_{3B})) \\ &+ c_A(1+\eta_{2A}-2\eta_{3A})\ln c_A(1+\eta_{2A}-2\eta_{3A}) \\ &+ c_B(1+\eta_{2B}-2\eta_{3B})\ln c_B(1+\eta_{2B}-2\eta_{3B}) \\ &+ (1-c_A(1+\eta_{2A}-2\eta_{3A})-c_B(1+2\eta_{2B} \\ &- 3\eta_{3B}))\ln(1-c_A(1+\eta_{2A}-2\eta_{3A}) \\ &- c_B(1+\eta_{2B}-2\eta_{3B}))\big] \\ &+ (k_BT/2)\big[c_A(1-\eta_{2A})\ln(c_A(1-\eta_{2A})) \\ &+ c_B(1-\eta_{2B})\ln(c_B(1-\eta_{2B})) \\ &+ (1-c_A(1-\eta_{2A})-c_B(1-\eta_{2B}))\ln(1 \\ &- c_A(1-\eta_{2A})-c_B(1-\eta_{2B}))\big] \end{aligned} \tag{13}$$

where $\mathbf{k}_2$ is the superlattice vector for the DO_{22} ordered phases given by $\mathbf{k}_2 = \pi(2\mathbf{a}_1^* + \mathbf{a}^*{}_3)$.

The free energy of the disordered phase can be obtained from (9) or (13) by letting the order parameters equal to zero, i.e.

$$F(\text{disordered}) = 1/2\big[(V_{BC}(\mathbf{0}) + V_{AC}(\mathbf{0}) - V_{AB}(\mathbf{0}))c_A c_B + V_{BC}(\mathbf{0})c_B^2 + V_{AC}(\mathbf{0})c_A^2\big] + k_B T\big[c_A \ln(c_A) + c_B \ln(c_B) + (1 - c_A - c_B)\ln(1 - c_A - c_B)\big] \quad (14)$$

In order to determine the equilibrium fields of the disordered phase (α), $L1_2$ and DO_{22}, i.e. the phase diagram of the pseudobinary Ni_3Al–Ni_3V system, we need to determine the interatomic interchange energies, $V^i_{\alpha\beta}$. They can be obtained either from first-principles calculations or by fitting them to the experimental phase diagram [6]. We chose to adopt the latter strategy and assumed a fourth nearest-neighbor interatomic model. The free energies of the $L1_2$ and DO_{22} ordered phases as a function of composition at a given temperature are, then, obtained by minimizing equations (9) and (13) with respect to their respective order parameters. Finally, the equilibrium compositions, or, the phase boundaries of the disordered phase, the $L1_2$ and DO_{22} ordered phases are determined numerically by the common tangent construction. The phase diagram obtained by using this procedure is shown in Fig. 1, with the available experimental points added in for comparison. It can be seen that a reasonably good fit is obtained using the following interaction parameters: for Ni and Al interactions (meV/atom), $V_1 = 122.30$, $V_2 = 6.0$, $V_3 = 16.58$ and $V_4 = -6.82$; for Ni and V interactions, $V_1 = 107.2$, $V_2 = 32.0$, $V_3 = -9.6$ and $V_4 = 12.8$; and for Al and V interactions, $V_1 = 40.0$, $V_2 = -30.0$, $V_3 = -80.0$ and $V_4 = 0.0$.

The instability lines of the high-temperature disordered phase with respect to ordering concentration waves with the superlattice vectors $\mathbf{k}_1$ and $\mathbf{k}_2$ of the $L1_2$ and DO_{22} phases are also shown in Fig. 1. It has been shown that the instability surface of an initial homogeneous disordered phase with respect to a concentration wave of wavenumber $\mathbf{k}$, is given by [7],

$$(k_B T)^2 + k_B T\big[V_{BC}(\mathbf{k})c_B c_C + V_{AC}(\mathbf{k})c_A c_C + V_{AB}(\mathbf{k})c_A c_B\big] + V_{AC}(\mathbf{k})V_{BC}(\mathbf{k})c_A c_B c_C - \frac{1}{4}(-V_{AB}(\mathbf{k}) + V_{AC}(\mathbf{k}) + V_{BC}(\mathbf{k}))^2 c_A c_B c_C = 0 \quad (15)$$

Although both $\mathbf{k}_2$ and $\mathbf{2k}_2$ are superlattice vectors for the DO_{22} phase, $\mathbf{2k}_2$ is equivalent to $\mathbf{k}_1$. The dash line labeled for the DO_{22} phase is the instability line of the disordered phase with respect to the ordering concentration wave with wave vector $\mathbf{k}_2$.

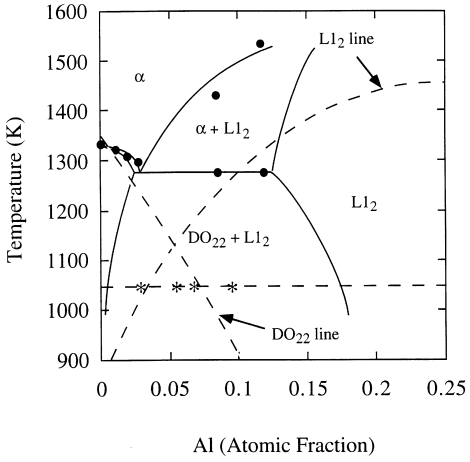

Fig. 1. The Al–V (Ni = 75%) pseudo-binary phase diagram (—), with the $L1_2$ ($\mathbf{k}_1$) and DO_{22} ($\mathbf{k}_2$) instability lines (- - -) superimposed. The experimental data is indicated by dots.

4. COMPUTER SIMULATIONS

To perform computer simulations of the atomic ordering and compositional clustering kinetics during the precipitation of $L1_2$ and DO_{22} ordered phases from a disordered phase, we have to numerically solve the kinetic equations for the single-site occupation probability functions. Since we employed a fourth-neighbor interaction model, it is convenient and even computationally advantageous to solve the kinetic equations in the reciprocal space. Fourier transforming both sides of the kinetic equation (1) gives

$$\frac{d\tilde{P}_A(\mathbf{k}, t)}{dt} = \tilde{L}_{AA}(\mathbf{k})/k_B T\Big\{\tilde{V}_{AC}(\mathbf{k})\tilde{P}_A(\mathbf{k}, t) + 1/2\Big[-\tilde{V}_{AB}(\mathbf{k}) + \tilde{V}_{BC}(\mathbf{k}) + \tilde{V}_{AC}(\mathbf{k})\Big]\tilde{P}_B(\mathbf{k}, t) + k_B T\Big\{\ln[P_A(\mathbf{r}, t)/(1 - P_A(\mathbf{r}, t) - P_B(\mathbf{r}, t)]\Big\}_{\mathbf{k}}\Big\} + \tilde{L}_{AB}(\mathbf{k})/k_B T\Big\{\tilde{V}_{BC}(\mathbf{k})\tilde{P}_B(\mathbf{k}, t) + 1/2[-\tilde{V}_{AB}(\mathbf{k}) + \tilde{V}_{BC}(\mathbf{k}) + \tilde{V}_{AC}(\mathbf{k})]\tilde{P}_A(\mathbf{k}, t) + k_B T\Big\{\ln[P_A(\mathbf{r}, t)/(1 - P_A(\mathbf{r}, t) - P_B(\mathbf{r}, t)]\Big\}_{\mathbf{k}}\Big\} \quad (16)$$

and

$$\frac{d\tilde{P}_B(\mathbf{k}, t)}{dt} = \tilde{L}_{BA}(\mathbf{k})/k_B T\Big\{\tilde{V}_{AC}(\mathbf{k})\tilde{P}_A(\mathbf{k}, t) + 1/2\Big[-\tilde{V}_{AB}(\mathbf{k}) + \tilde{V}_{BC}(\mathbf{k}) + \tilde{V}_{AC}(\mathbf{k})\Big]\tilde{P}_B(\mathbf{k}, t) + k_B T\Big\{\ln[P_A(\mathbf{r}, t)/(1 - P_A(\mathbf{r}, t) - P_B(\mathbf{r}, t)]\Big\}_{\mathbf{k}}\Big\}$$

$$+\tilde{L}_{BB}(\mathbf{k})/k_B T\Big\{\tilde{V}_{BC}(\mathbf{k})\tilde{P}_B(\mathbf{k},t)$$
$$+1/2[-\tilde{V}_{AB}(\mathbf{k})+\tilde{V}_{BC}(\mathbf{k})$$
$$+\tilde{V}_{AC}(\mathbf{k})]\tilde{P}_A(\mathbf{k},t)+k_B T$$
$$\Big\{\ln[P_A(\mathbf{r},t)/(1-P_A(\mathbf{r},t)-P_B(\mathbf{r},t)]\Big\}_{\mathbf{k}}\Big\}$$

where $\{\ln[P_A(\mathbf{r},t)/(1-P_A(\mathbf{r},t)-P_B(\mathbf{r},t))]\}_{\mathbf{k}}$, $\{\ln[P_B(\mathbf{r},t)/(1-P_A(\mathbf{r},t)-P_B(\mathbf{r},t))]\}_{\mathbf{k}}$, $\tilde{P}_A(\mathbf{k},t)$, $\tilde{P}_B(\mathbf{k},t)\tilde{L}_{AA}(\mathbf{k})$, $\tilde{L}_{AB}(\mathbf{k})$, $\tilde{L}_{BA}(\mathbf{k})$, and $\tilde{L}_{BB}(\mathbf{k})$ are Fourier transforms of corresponding functions in the real space. By assuming atomic jumps between nearest neighbor sites only and using the condition that the total number of atoms in the system are conserved, for an f.c.c. lattice, we can write

$$\tilde{L}_{\alpha\beta}(\mathbf{k}) = -4L_0^{\alpha\beta}[3-\cos\pi h\cdot\cos\pi k - \cos\pi k\cdot\cos\pi l-\cos\pi l\cdot\cos\pi h] \quad (17)$$

where $L_0^{\alpha\beta}$ is proportional to the jump probability between a pair of atoms α and β at nearest-neighbor sites per unit time.

Although it is straightforward and desirable to perform three-dimensional simulations using the microscopic diffusion equations outlined above, a two-dimensional simulation is much less computationally intensive, and the analysis and visualization of the atomic configuration and multiphase morphologies are much easier. As a result, all the results reported in this paper were obtained using two-dimensional projections of a three-dimensional system. It is equivalent to assuming that the occupation probabilities do not depend on the coordinate z along the [001] axis. The formulation of the kinetic equations on a two-dimensional projection of a three-dimensional f.c.c. lattice presented below was originally suggested by Khatchaturyan in a private communication.

The two-dimensional projection of a f.c.c. lattice along the [001] direction, is a square lattice whose lattice parameter is half of that of the F.C.C. lattice. Therefore, a lattice vector $\mathbf{r}$ in the two-dimensional square lattice can be written as

$$\mathbf{r} = x'\mathbf{b}_1 + y'\mathbf{b}_2 = \frac{x'}{2}\mathbf{a}_1 + \frac{y'}{2}\mathbf{a}_2 \quad (18)$$

where $\mathbf{b}_1$ and $\mathbf{b}_2$ are unit cell vectors of the square lattice, and $\mathbf{a}_1$ and $\mathbf{a}_2$ are the unit cell vectors of the f.c.c. lattice on the projected plane. The corresponding reciprocal lattice vector $\mathbf{k}$ for the square lattice is

$$\mathbf{k}' = 2\pi(h'\mathbf{b}_1^* + k'\mathbf{b}_2^*) = 2\pi(2h'\mathbf{a}_1^* + 2k'\mathbf{a}_2^*) \quad (19)$$

where $\mathbf{b}_1^*$ and $\mathbf{b}_2^*$ are the corresponding reciprocal unit cell vectors for the square lattice, and $\mathbf{a}_1^*$ and $\mathbf{a}_2^*$ are the reciprocal unit cell vectors for the lattice defined by the real space unit cell vectors, $\mathbf{a}_1$ and $\mathbf{a}_2$.

Therefore, on the projected two-dimensional square lattice, the kinetic equations in the reciprocal space are obtained by substituting $(2h', 2k', 0)$ for (h, k, l) in equations (12) and (17) with

$$V(\mathbf{k}') = 4W_1(\cos 2\pi h'\cdot\cos 2\pi k' + \cos 2\pi h' + \cos 2\pi k') + 2W_2(\cos 4\pi h' + \cos 4\pi k' + 1) + \cdots \quad (20)$$

and

$$\tilde{L}_{\alpha\beta}(\mathbf{k}') = -4L_0^{\alpha\beta}[3-\cos 2\pi h'\cdot\cos 2\pi k' - \cos 2\pi k' - \cos 2\pi h'] \quad (21)$$

The projected $L1_2$ and DO_{22} ordered structures are shown in Fig. 2 for reference.

In the simulation, the coefficients $L_0^{\alpha\beta}$ are chosen with the condition that the matrix has to be positive definite. In particular, we chose

$$L_0^{\alpha\beta} = \begin{bmatrix} 1 & -0.5 & -0.5 \\ -0.5 & 1 & -0.5 \\ -0.5 & -0.5 & 1 \end{bmatrix} \quad (22)$$

We also tested other values of the coefficients and we found that the results on the ordering kinetics obtained from computer simulations, in particular, the ordering sequence, seem to be quite insensitive to the exact values chosen for these coefficients, as long as the matrix is positive definite. The kinetic equations were solved using the explicit forward Euler technique.

We first tested the equilibrium phase diagram by performing computer simulations in various single- and two-phase fields in the pseudobinary phase diagram including the two-phase fields of $\alpha + L1_2$ above the eutectoid and $L1_2$ and DO_{22} single-phase fields. The structures, compositions, and the equilibrium volume fractions as well as the ordering instability lines of both ordered phases obtained from the computer simulation are consistent with the calculated phase diagram. For example, our

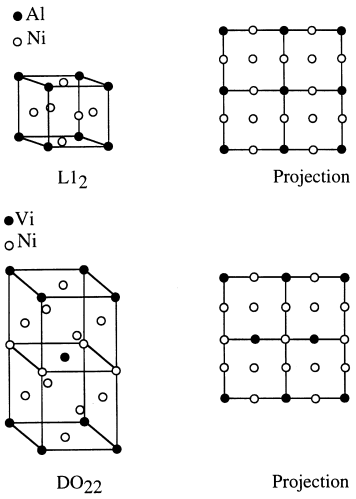

Fig. 2. The $L1_2$ and DO_{22} structures and their projections.

computer simulations demonstrated that a disordered phase annealed in the two-phase ($\alpha + L1_2$) region on the calculated phase diagram transforms into a two-phase microstructure consisting of $L1_2$ particles embedded in a disordered matrix, and the compositions of the two phases match the equilibrium compositions predicted by the phase diagram. We also calculated the variation of the two order parameters in the DO_{22} phase with temperature at a composition close to the Ni_3V stoichiometry (Fig. 3) from the occupation probabilities at each site obtained from the kinetic computer simulations and the transition temperatures obtained seem to agree with the equilibrium phase diagram calculation as well.

Our focus of this paper is on the kinetics of atomic ordering and clustering during precipitation of both $L1_2$ and DO_{22} ordered phases from the disordered matrix. We chose a temperature of 1046.5 K which is close to that employed in experiments [2] and examine the kinetics of diffusional precipitation during the annealing of a disordered phase at various compositions of $c_{Al} = 0.03$, 0.04, 0.055, 0.07 and 0.08 atomic fraction. All these compositions are in the two-phase field containing both $L1_2$ and DO_{22} at 1046.5 K. The initial disordered phase was generated by assigning the average compositions of Ni, Al and V to the respective occupation probability functions at each lattice site. Within the two-phase field of $L1_2 + DO_{22}$, the initial single-site occupation probability functions describing the disordered state are non-equilibrium, and with some small random perturbations, they evolve as a function of time and their temporal evolution describes the kinetics of atomic ordering and compositional clustering.

Figure 4(a) shows the morphological evolution of the alloy with the composition $c_{Al} = 0.03$, at different time steps. The color scheme used to depict the pictures is as follows: the color assigned to each lattice site is a mixture of red, green and blue, in the same proportion as the ratios of the occupation probability at that site of aluminum, vanadium and nickel, respectively. Thus, if the occupation probability of aluminum at any site is 1.0, then that site is assigned the color red, and so on. The DO_{22} phase therefore appears as green, since the dominating color at the vanadium sites is green. Similarly, the $L1_2$ phase appears as red. All the nickel sites in both phases appear as blue, which, therefore, seems to form a background color. It can be seen that the initial stage of annealing of the disordered state involves atomic ordering in the disordered state resulting in the formation of DO_{22} domains separated by antiphase domain boundaries (APBs). Notice that the V atoms are arranged in a hexagonal fashion (it is not truly hexagonal since not all sides have the equal length), consistent with a projection of the DO_{22} structure. Accompanying the formation and growth of DO_{22} ordered domains, Al atoms start to segregate to the APBs of the DO_{22} ordered phase while the V atoms deplete from the APBs. As the degree of Al segregation at the antiphase domain boundaries increases, the $L1_2$ ordered domains started to nucleate and grow at the APBs of the DO_{22} ordered phase. The $L1_2$ ordered domains can be identified by the Al sites arranged in a square lattice consistent with the projection of the cubic $L1_2$ phase shown in Fig. 2. After the formation of an equilibrium two-phase mixture of $L1_2$ and DO_{22} ordered domains, the subsequent process is mainly domain coarsening (of course, some coarsening also took place even before the formation of the equilibrium two-phase mixture). Close examination of the amounts of the two phases present, as well as the composition of the two phases, show that they are consistent with the phase diagram. The information on the sequence of DO_{22} and $L1_2$ ordering can also be obtained from the diffraction patterns of the microstructures, which are embedded within the frames of Fig. 4(a). The diffraction pattern of the $L1_2$ phase is obtained from the square of the Fourier transform of the occupation probabilities of Al atoms, while the diffraction pattern of the DO_{22} phase is obtained from the square of the Fourier transform of the occupation probabilities of V atoms. On the 2-D projection, the superlattice vectors of $L1_2$ ordered phase are located at (h', k') = (0,1), (1,0) and (1,1) while those of the DO_{22} ordered phase occur at (1/2.1), (1,1/2), (3/2,1) and 1,3/2). The diffraction intensities are represented using grey-levels. The diffraction pattern of the $L1_2$ phase is shown in the lower left inset and that of the DO_{22} is in the upper right inset. It can be seen that the superlattice reflections corresponding to the DO_{22} order appear before $L1_2$. The time-dependence of the intensity of the $L1_2$ and DO_{22} superlattice reflections is plotted in Fig. 5(a), which indicates quite clearly that DO_{22} ordering takes place before $L1_2$. The kinetics of ordering of a disordered phase at $c_{Al} = 0.04$ or

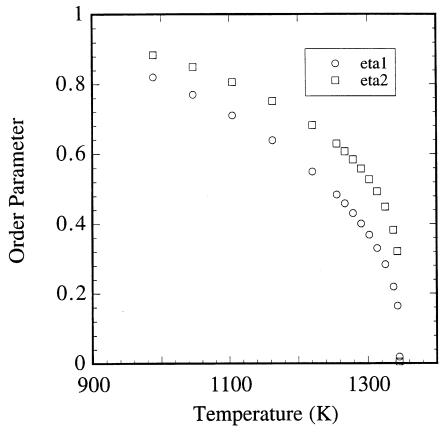

Fig. 3. The variation of the DO_{22} order parameters with temperature.

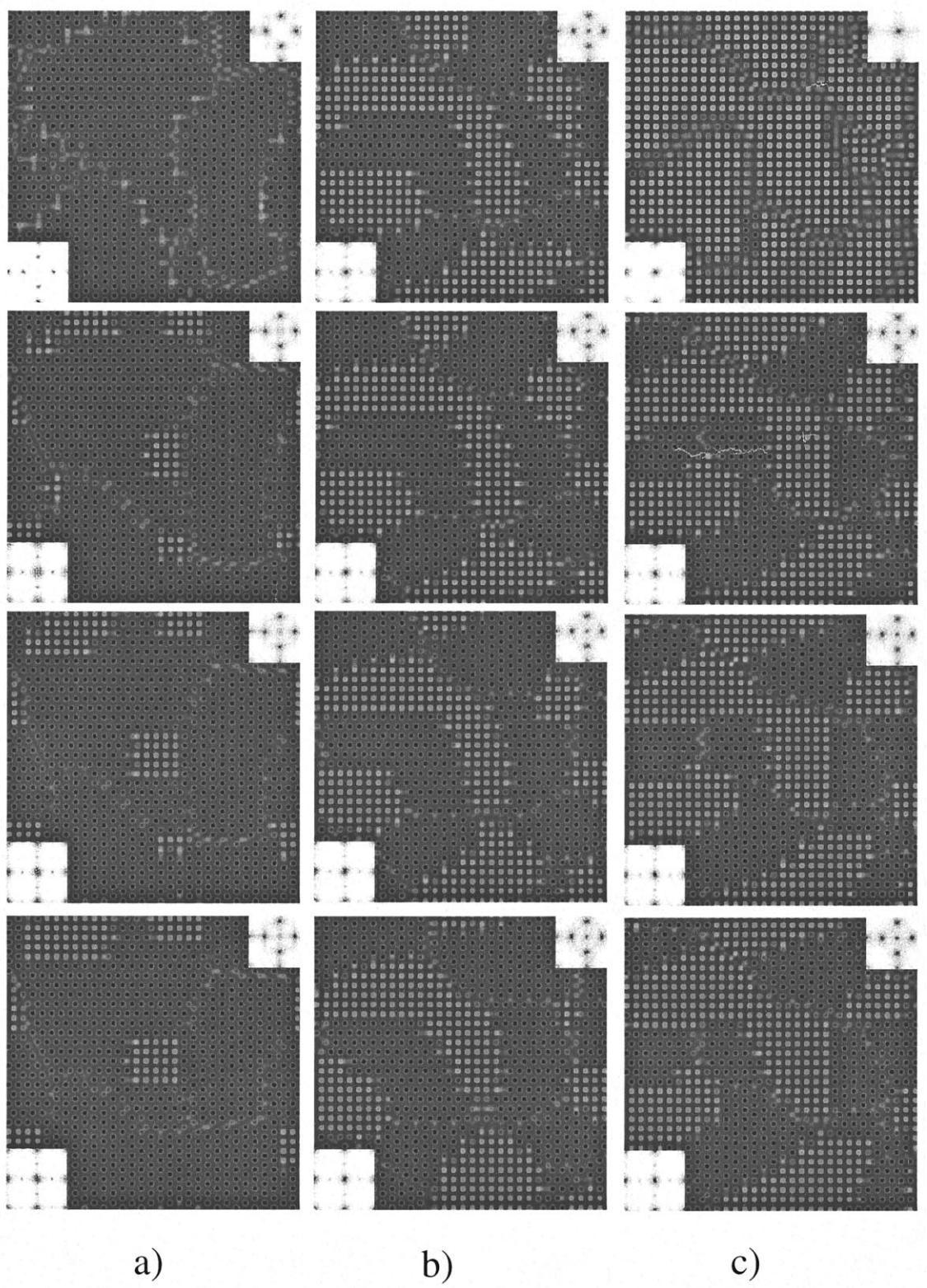

Fig. 4. Microstructural evolution at timestep $t^* = 5000$, 25,000, 50,000 and 100,000 for (a) Al = 0.03, (b) Al = 0.055 and (c) Al = 0.07.

$c_{Al}=0.05$ are very similar to that of $c_{Al}=0.03$, except that the $L1_2$ phase formed at successively earlier times, indicating increased ease of formation of $L1_2$, which is consistent with the fact that with increasing Al composition, the driving force for the formation of the $L1_2$ phase increases.

Figure 4(b) shows the temporal evolution of the microstructure for $c_{Al}=0.055$, and it can be seen that at this composition, both the DO_{22} and the $L1_2$ phase form practically simultaneously. The microstructure contains both phases even from very early times, and the diffraction patterns also reflect this same information. Figure 5(b) shows the temporal growth in the intensity of the diffraction spots, showing practically simultaneous growth of both phases. As we will discuss later, the main reason for the simultaneous growth of $L1_2$ and DO_{22} ordered domains is that driving forces for the formation of the two phases are almost equal.

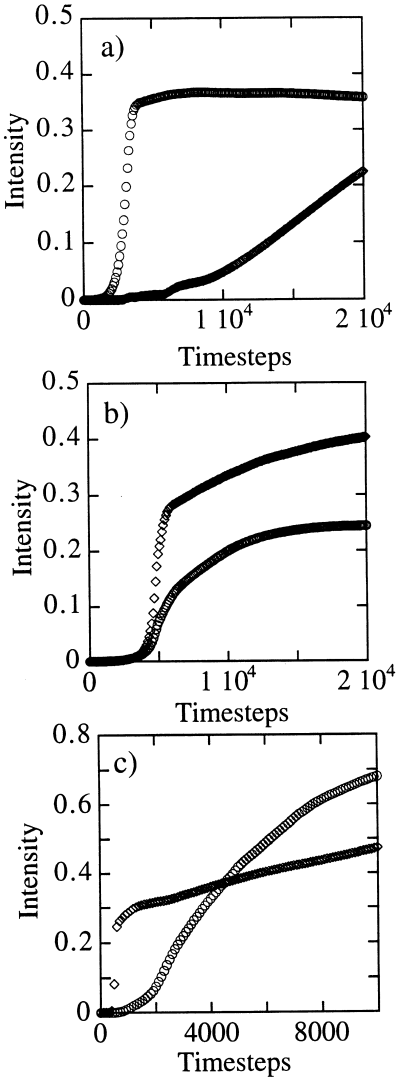

Fig. 5. The temporal growth of the diffraction intensities of the $L1_2$ and DO_{22} phases, for (a) Al = 0.03, (b) Al = 0.055 and (c) Al = 0.07.

As the composition is increased to $c_{Al}=0.07$ [see Fig. 4(c) and 5(c)], the sequence in which the two phases form is reversed. The $L1_2$ phase now forms first, followed at later times by the formation of the DO_{22} phase at the anti-phase domain boundaries of the $L1_2$ phase. At $c_{Al}=0.08$, The same sequence is observed, with the DO_{22} phase forming with greater difficulty, i.e. at later times than at $c_{Al}=0.07$.

Most of the compositions discussed above (Al = 0.055 and Al = 0.07) are below the instability lines of both the $L1_2$ and DO_{22} ordered phases. However, we found that even when the composition is below one of the instability lines and above the other, the kinetics of ordering and compositional clustering processes appear to be consistent with the above scheme that below $c_{Al}=0.055$, the DO_{22} domains appear first, while above $c_{Al}=0.055$, the $L1_2$ domains appear first. For example, Fig. 6 shows the microstructural evolution for a system at Al = 0.10 and T = 1046.5 K (i.e. above the DO_{22} stability line), as a function of time. It is clear that for $c_{Al}=0.10$, the $L1_2$ ordering still precedes DO_{22}. As this composition is above the ordering instability line of the DO_{22} phase, the initial disordered state is metastable with respect to ordering to the DO_{22} phase. The kinetic equation (1) are deterministic and hence cannot describe processes which require thermal fluctuations, such as nucleation of ordered domains in a metastable state. Therefore, one of the reasons that $L1_2$ ordering takes place first before DO_{22} order might be due to the fact that the initial disordered state is metastable with respect to DO_{22} ordering, and the fact that the kinetic equations cannot describe the nucleation process. In order to examine if this is the case, we introduced a random noise term, $\xi(\mathbf{r},t)$, to the right-hand sides of the kinetic equation (1), to simulate the thermal fluctuations. The noise term is assumed to be Gaussian-distributed with average zero, and uncorrelated with respect to both space and time [8–10]. The value for the variance of the noise was introduced rather arbitrarily, to ensure nucleation within a reasonable simulation time, so it is important to point out that the nucleation rate described by the noise term is incorrect. Nevertheless, the noise term introduced in such an *ad hoc* way does result in nucleation, as we discuss below for the case of compositions above both the ordering instability lines. With thermal noise, DO_{22} ordered domains appear at an earlier time compared to the simulation without thermal noise. However, the thermal noise does not change the sequence of ordering, i.e. $L1_2$ ordering precedes DO_{22} order and the DO_{22} ordered domains nucleated at the APBs of the $L1_2$ ordered phases.

When a composition is above the ordering instability lines of both $L1_2$ and DO_{22}, but within the two-phase field, according to thermodynamics,

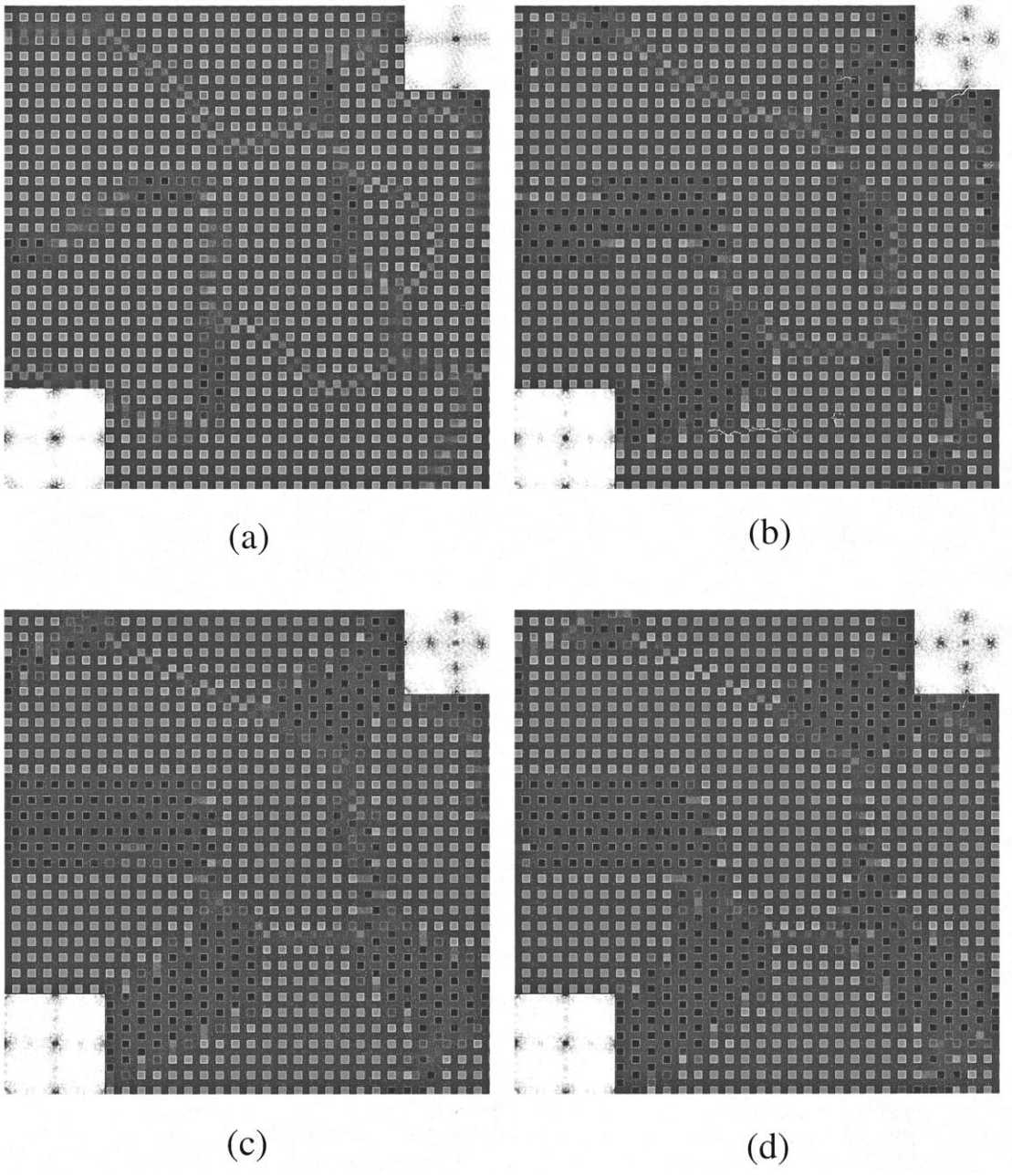

Fig. 6. The microstructural evolution for $c_{Al} = 0.10$ at different timesteps.

the ordered phase can only form through a nucleation and growth process, since the initial disordered state is metastable with respect to both $L1_2$ ordering and DO_{22} ordering. Indeed, our computer simulation shows that initial small random perturbations actually decay and the initial disordered phase remains in its metastable state indefinitely. In order to promote nucleation of ordered domains, again, we added Langevin noise terms to the right-hand sides of the microscopic diffusion equations. We found that the $L1_2$ and DO_{22} phases appear almost simultaneously during a computer simulation with the noise terms.

5. DISCUSSION

Our computer simulations demonstrated that when c_{Al} is smaller than the crossover composition, 0.055, of the ordering instability lines with respect to the $L1_2$ and DO_{22} phases on the pseudobinary Ni_3Al–Ni_3V diagram, the first stage of phase transformation during the annealing of a disordered phase annealed in the two-phase field of $L1_2 + DO_{22}$, involves DO_{22} ordering, followed by the appearance of $L1_2$ ordered domains at the APBs of the DO_{22} phase. On the other hand, if the c_{Al} is larger than 0.055, the first stage is the $L1_2$

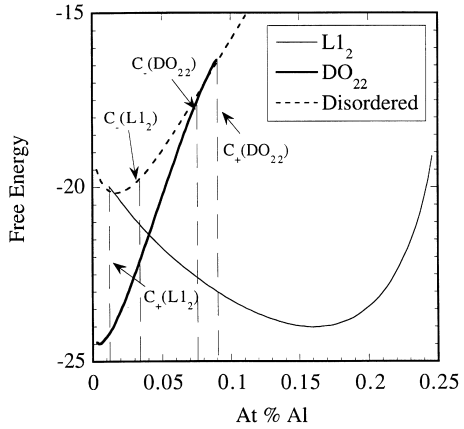

Fig. 7. The free energy-composition curves obtained at $T = 1046.5$ K.

ordering preceding the formation of DO_{22} ordered domains at the APBs of the $L1_2$ domains. For compositions close to 0.055, $L1_2$ and DO_{22} ordered domains appear simultaneously. These results are consistent with the experimentally observations by Bendersky *et al.* [2] in the system.

The ordering sequences of $L1_2$ and DO_{22} phases at other temperatures are similar to those at 1046.5 K although the kinetic mechanism of ordering may be different at different temperatures, i.e. $L1_2$ and DO_{22} order can take place either continuously or by a nucleation and growth mechanism. Since the diffusion distances required for ordering of a disordered phase into both $L1_2$ and DO_{22} are similar, on the order of interatomic distances, it is clear that the difference in the rates of ordering at different compositions must be due to the difference in their driving forces. This should be true, in general, for precipitation of any two ordered phases from a disordered matrix. Results of our computer simulations indicate that the undercooling with respect to the ordering instability lines of the two phases is a good measure of the driving forces for the formation of the corresponding ordered phases.

We have to distinguish the driving forces for the development of a local fluctuation of long-range order and a global one. Figure 7 shows the free energy-composition curves of the pseudobinary Ni_3Al–Ni_3V system at $T = 1046.5$ K, which was chosen to be the temperature at which most of the simulations were performed. From Fig. 7, it is easy to see that the final equilibrium state is a mixture of two ordered phases, $L1_2$ and DO_{22} with equilibrium composition, $c_{Al} = 0.008$, for the DO_{22} phase and $c_{Al} = 0.17$ for the $L1_2$ phase determined from the common tangent. By definition, the global driving force is defined as the free energy difference between the final state and the initial state. According to Fig. 7, the aluminum composition at which the free energy curves for $L1_2$ and DO_{22} intersect is about 0.045, and hence the global driving forces for the transformation of a single-phase disordered state to a single-phase $L1_2$ ordered state and to a single-phase DO_{22} ordered state are equal at $c_{Al} = 0.045$. Yet, our computer simulations demonstrated that at this composition, DO_{22} ordered domains appear before $L1_2$. Therefore, the magnitude of the global driving force is not a good measure for determining the sequence of $L1_2$ and DO_{22} ordering. On the other hand, the driving force for the development of a local long-range order fluctuation, $\delta\eta(r)$, is related to the second-derivatives of the free energy with respect to the corresponding long-range order parameter, i.e.

$$\Delta f \sim \int (\partial^2 f/\partial \eta^2)_{\eta=0} (\delta\eta)^2 d^3 r \sim C(T - T_-) \int (\delta\eta)^2 d^3 r \tag{23}$$

where C is a constant and T_- is the ordering instability temperature below which the $(\partial^2 f/\partial \eta^2)_{\eta=0}$ is negative. Therefore, it is the driving force for local long-range order fluctuation which is relevant to the rate of ordering. Equation (23) also shows that the driving force for local fluctuation is proportional to the undercooling below the ordering instability line, $(T - T_-)$. At $T = 1046.5$ K, the disordered phase is unstable throughout the whole two-phase composition range. For all compositions below $c_{Al} = 0.075$, the disordered phase is unstable with respect to the DO_{22} phase, while at all compositions greater than $c_{Al} = 0.032$, it is unstable with respect to the $L1_2$ phase. Thus, between $c_{Al} = 0.075$ and $c_{Al} = 0.032$, the disordered phase is unstable with respect to both ordered phases. At compositions close to $c_{Al} = 0.055$, the ordering instability lines for $L1_2$ and DO_{22} intersect, and hence the driving forces for the development of local long-range $L1_2$ and DO_{22} order at $c_{Al} = 0.055$ are very similar. Therefore, it is expected that $L1_2$ and DO_{22} ordered domains appear simultaneously from a disordered matrix. If the initial composition of the disordered phase is much larger than $c_{Al} = 0.055$, then $L1_2$ is expected to precipitate first because of the fact that disordered phase is absolutely unstable with respect to $L1_2$ and metastable with respect to DO_{22} and also the fact that the driving force for $L1_2$ ordering is larger than for DO_{22}. On the other hand, if the composition is much smaller than $c_{Al} = 0.055$, DO_{22} ordering will precede $L1_2$. This qualitative analysis is consistent with our computer simulations.

After the formation of equilibrium two-phase mixture of $L1_2$ and DO_{22} ordered phases, the subsequent process is primarily domain coarsening. It should be pointed out that domain coarsening in such a two-phase mixture is very interesting in the sense that domain growth through APB (boundaries between different antiphase $L1_2$ ordered domains or those between DO_{22} ordered domains) migration and Ostwald ripening via interphase boundary (the

boundaries between an $L1_2$ domain and a DO_{22}) motion take place simultaneously. The situation is very similar to the case of coupled grain growth and Ostwald ripening in a polycrystalline two-phase solid. The diffusion distance involved in an APB migration is on the order of APB width whereas the diffusion distance involved in an interphase boundary motion is on the order of the separation distance of second-phase particles. In the case of polycrystalline two-phase solids, we show that [11] although grain growth and Ostwald ripening occur simultaneously, the overall grain growth rate is controlled by long-range diffusion, i.e. Ostwald ripening, with the average grain size varies as a function of time as $t^{1/3}$. It may be expected that it is also the case here for the domain coarsening of a $L1_2$ and DO_{22} two-phase mixture.

6. CONCLUSION

The kinetics of atomic ordering and compositional clustering process during the phase transformation of an initially homogeneous disordered f.c.c. ternary alloy ($Ni_{75}Al_{25-x}V_x$) into a two-phase mixture of $L1_2(Ni_3Al)$ and $DO_{22}(Ni_3V)$ ordered phases were investigated using computer simulations based on microscopic diffusion equations. Our computer simulations demonstrated that at small Al content (less than $c_{Al}=0.055$), the DO_{22} ordered domains appear first, followed by the nucleation of $L1_2$ ordered domains at the antiphase domain boundaries of DO_{22}, whereas at large Al content (larger than $c_{Al}=0.055$), precipitation of $L1_2$ domains precedes DO_{22} phase formation. It is shown that the rate of ordering for $L1_2$ and DO_{22} are mainly determined by their thermodynamic driving forces for local long-range order, which is linked to the undercooling with respect to the ordering instability lines of the two phases. $L1_2$ and DO_{22} ordering may take place either through a continuous mechanism due to the thermodynamic instability of the parent disordered phase, or a nucleation and growth mechanism. The ordering sequence predicted from our computer simulation agrees with recent experimental observations on the alloys.

Acknowledgements—The work is supported by the Office of Naval Research Young Investigator Program under the grant number N-00014-95-1-0577 and by the ARPA/NIST program on mathematical modeling of microstructure evolution in advanced alloys. Computation time was provided through a grant of HPC time from the DoD HPC Center, CEWES, on the C90.

REFERENCES

1. Hong, Y. M., Nishima, Y. and Suzuki, T., *Mat. Res. Soc. Symp. Proc.*, 1989, **133**, 429.
2. Bendersky, L. A., Biancaniello, F. S. and Williams, M. E., in *Solid-Solid Phase Transformations*, ed. Johnson W. C., Howe J. M., Laughlin D. E. and Soffa W. A. TMS, Warrendale, PA, 1994, p. 899.
3. Soffa, W. A. and Laughlin, D. E., *Acta Metall.*, 1989, **37**, 3019.
4. Chen, L-Q., *Scripta Metall.*, 1993, **29**, 683.
5. Khachaturyan A. G., *Theory of Structural Transformations in Solids*. Wiley, New York, 1983; Khachaturyan A. G., *Sov. Phys. Solid State*, 1968, **9**, 2040.
6. Khachaturyan, A. G., Lindsey, T. F. and Morris, J. W., *Metall. Trans.*, 1988, **19A**, 249.
7. Chen, L-Q., *Acta Metall.*, 1994, **42**, 3503.
8. Wang, Y., Chen, L-Q. and Khachaturyan, A. G., in *Solid-> Solid Phase Transformations*, ed. Johnson W. C., Howe J. M., Laughlin D. E. and Soffa W. A. TMS-AIME, Warrendale, PA, 1994 p. 245.
9. Keng Ma, Shang, *Modern Theory of Critical Phenomena*, W.A. Benjamin Inc., Reading, MA, 1976.
10. (a) Siegert M., Madan Rao, *Phys. Rev. Lett.*, 1956, **70**, 1956, (b) Rogers T. M., Elder K. R. and Desai R. C., *Phys. Rev. B*, 1988, **37**, 9638.
11. Chen L.-Q., Fan D., *J. Am. Ceram. Soc.*, 1996, **79**, 1163; Fan D., Ph.D. thesis, Penn State University, 1996.